AN ABSTRACT OF THE THESIS OF

Nichole D. Sullivan for the degree of Honors Baccalaureate of Science in Bioresource Research presented on March 17, 2009. Title: Two advances in practical alternative energy: thermotolerant hydrogenase concentration and methane hydrate grain size proxies.

Abstract approved: _____
Anne Trehu

Methane hydrates and biohydrogen are two disparate subjects that are of interest in the growing field of alternative energy research. However, before commercial use becomes a viable option, each has challenges that need to be overcome. Methane hydrates require large investments of time and capital to locate. In this thesis, physical properties of marine sediments were evaluated to determine if they could serve as useful proxies for grain size, which has been proven to correlate to the presence of methane hydrates in marine sediments. Grain size was manually analyzed for a set of over 600 marine sediment samples using wet-sieving and compared to a defined set of sediment parameters. Of the parameters analyzed, none proved successful proxies for grain size. Biohydrogen is hydrogen that is biologically produced, usually by bacteria, and has the potential to be used in fuel cells with currently available technology. The main barrier to commercial production is the sensitivity of hydrogen-producing hydrogenase enzymes to heat and oxygen. In this thesis, a particularly heat- and oxygen-stable hydrogenase enzyme, *hynSL*, was isolated from the phototrophic purple sulfur bacterium *Thiocapsa roseopersicina* and concentrated.

Key Words: Alternative energy, methane hyrates, grain size proxies, biohydrogen, *Thiocapsa roseopersicina*, hydrogenase, *hynSL*

Corresponding email address: cespeden@onid.orst.edu

Two advances in practical alternative energy: thermotolerant hydrogenase concentration and methane hydrate grain size proxies.

by

Nichole D. Sullivan

A PROJECT

submitted to

Oregon State University

University Honors College

in partial fulfillment of
the requirements for the
degree of

Honors Baccalaureate of Science in BioResource Research

Presented March 17, 2009
Commencement June 2008

Honors Baccalaureate of Science in BioResource Research project of Nichole D. Sullivan presented on March 17, 2009.

APPROVED:

Mentor, representing College of Oceanic and Atmospheric Science

Secondary mentor, representing Biological and Ecological Engineering

Committee Member, representing College of Agricultural Sciences

Director, BioResource Research

Dean, University Honors College

I understand that my project will become part of the permanent collection of the Oregon State University Library, and will become part of the Scholars Archive collection for Bioresource Research. My signature below authorizes release of my project to any reader upon request.

Nichole D. Sullivan, Author

TABLE OF CONTENTS

LIST OF FIGURES

LIST OF TABLES

ACKNOWLEDGEMENTS

I would like to thank Anne Trehu for her patience, professionalism and guidance. I am a better researcher because of it. I am grateful to Roger Ely for the opportunity to work in his lab. I'd like to thank Jed Eberly, Hatem Mohamed, and Liz Burrows in the Ely lab for their patience, advice and support. I am also grateful to Jim Power for all his help, and the U.S. Environmental Protection Agency in Newport, OR for the use of the Laser Diffraction Particle Size Analyzer. I would like to thank the Arp lab for the use of the ultracentrifuge, and Luis Savayedra-Soto for his assistance and guidance. I would also like to thank my additional committee members, Cary Green and Kate Field, for their help and support in the writing (and re-writing) process. Special thanks to Wanda Crannell, the most amazing academic and personal advisor in the University system, without whom none of this work would have been completed in the first place.

Thank you to the Oregon Sea Grant and the Undergraduate Research, Innovation, Scholarship and Creativity (URISC) program for funding my research projects, and to the Integrated Ocean Drilling Program (IODP) for research funding and supporting my travel to the American Geophysical Union Fall 2006 conference.

Finally, thanks to my husband, family and friends for their prayers, support and encouragement throughout my entire education.

OVERVIEW

Finding a source of clean, efficient energy is one of the most important issues of our time. The global issues facing the world, identified in part by the United Nations and listed on their annual agenda (17), all require adequate energy to research and implement solutions. It is clear that this energy cannot continue to come from fossil fuels alone. Although debate continues over whether an oil shortage really exists, fossil fuel use in general has been widely implicated as a cause of global climate change (4, 5). For this reason, alternative energy is rapidly becoming one of the largest and most important research topics and industrial development opportunities in the world.

This thesis focuses on two promising alternative energy sources: biologically produced hydrogen (biohydrogen) (Chapter 1) and methane hydrates (Chapter 2).

Biohydrogen can be produced by the BBS strain of the purple sulfur bacterium *Thiocapsa roseopersicina*, isolated from the North Sea (10). *T. roseopersicina* contains hydrogenase enzymes that catalyze the interconversion of hydrogen gas (H_2) and its elementary particle constituents, two protons and two electrons (1). Hydogenase enzymes may be sensitive to a number of denaturing factors, including heat (6, 18) and pH (18). However, one of the major barriers to industrial levels of H_2 production and subsequent practical use is the high sensitivity of hydrogenase to oxygen. The hydrogenases from *T. roseopersicina* are unique in that they have a high heat tolerance, are resistant to proteolysis and have unusual oxygen stability (9). The research detailed in Chapter 1 focuses on the concentration of a membrane-associated hydrogenase of *T. roseopersicina* for future use in industrial hydrogen production applications.

Methane hydrate is a cage-like lattice of ice inside of which are trapped molecules of methane, the chief constituent of natural gas (3). The methane may be biological or geological in origin. Under the correct temperature and pressure conditions, methane present in marine sediments above methane saturation in the pore water forms hydrates. Methane hydrates can form in any environment where conditions are suitable and enough methane is present, but are mostly found under Arctic permafrost and in marine sediments on continental margins. Sediment grain size has been proven to correlate to methane hydrate presence (15). The research in Chapter 2 focuses on finding proxies for grain size in marine sediments.

Around the world, private companies and countries alike, including the United States through the Department of Energy (DOE), are devoting resources to methane hydrate research and exploration. According to the DOE, two major constraints to production are: 1) the need to detect and quantify methane hydrate deposits prior to drilling, and 2) the demonstration of methane production from hydrate at commercial volumes (3). Determination of successful grain size proxies would allow for less expensive and time-intensive location of methane hydrates using easily-measured sediment properties. Finding reliable proxies for grain size that are more easily measured would allow incorporation of borehole data into models of geological history and thus lead to better predictive models of where hydrate may be present. It would also facilitate research of marine sediment that uses sediment properties as proxies for grain size to interpret paleo-climate (11) and paleo-earthquake (7) data.

CHAPTER 1: CONCENTRATION OF A THERMOTOLERANT HYDROGENASE FOR PRODUCTION OF BIOHYDROGEN

Introduction

Hydrogen (H_2) is an ideal form of energy for several reasons. Hydrogen doesn't pollute the atmosphere or environment with typical fossil fuel byproducts because it isn't bound to carbon. In addition, hydrogen has a high energy to weight ratio, and can be used with currently available technology like internal combustion engines and fuel cells. Using hydrogen as an energy source would decrease dependence on current hydrocarbon fuel sources, a desirable goal as fossil fuel reserves decline and energy costs escalate.

Hydrogenase is an enzyme that metabolizes biological hydrogen. It can catalyze both H_2 generation (e.g. photobiological and fermentative) and H_2 oxidation (e.g. in fuel cells) (10). Most hydrogenases become inactivated fairly rapidly in the presence of oxygen and heat. However, thehydrogenases from the purple sulfur phototrophic bacterium *Thiocapsa roseopersicina* show surprisingly high stability against oxygen and heat (6). These hydrogenases may be membrane-bound, membrane-associated, or cytosolic. The hydrogenases of *T. roseopersicina* show high resistance to a variety of denaturing agents and show high stability to storage under various conditions (6). These hydrogenases are also characterized by high H_2 production rates (8). One hydrogenase in particular, *hynSL*, is remarkable because it remains active even after removal from the membrane, a promising characteristic for commercial hydrogen production, currently limited by the time and resource demands of batch cell cultivation. *HynSL* has a dinuclear catalytic center of nickel and iron (NiFe) (2) and can remain active at 80°C (176° F) for up to 10 days (10).

The main barrier to industrial-level H_2 production is the high sensitivity of hydrogenase to O_2. With the relatively stable hydrogenase of *T. roseopersicina*, such industrial H_2 production may lead to a viable and economically feasible hydrogen energy future. Studies on the purification procedures of hydrogenase are relatively limited (8). The goal of this project was to concentrate and characterize the *hynSL* hydrogenase enzyme of *T. roseopersicina*.

Materials and Methods

Growth of the organism

T. roseopersicina was grown in a 20-liter bioreactor using Pfennig's medium in a constant-temperature room under continuous light at 30 μE m^{-2} s^{-1}. The culture was purged with N_2 and sealed after initial inoculation and feedings. The culture was fed with 61 mM Na acetate. After 3 weeks, the culture was harvested by spinning at 17,700 × *g* and 4°C for 10 minutes. Harvested cells were frozen at -20°C for future use.

Membrane isolation

Frozen cells were resuspended in a 1:3 ratio with Buffer A (50 mM Tris at pH 8.0 containing 4 mM sodium dithionite) (12). The cell suspension was vortexed in three cycles of 30 seconds at the "homogenize" setting, 2 minutes resting to lyse cells (Mini-Beadbeater, Biospec Products, Bartlesville, OK, USA). The suspension was centrifuged at 2,000 × *g* for 30 seconds to pellet the beads. The cell suspension solution was removed and frozen at -20°C.

Cell debris was removed by centrifugation (28,000 × *g*, 4°C, 20 min). The cell extract was further ultra-centrifuged (300,000 × *g*, 4°C, 1h) to prepare the cytoplasmic fraction, which was frozen for further use (8).

Concentration of Hydrogenase

The frozen cytoplasmic fraction was thawed at 4°C and precipitated overnight at 60% ammonium sulfate saturation. The fraction was centrifuged (10,000 rpm, 4°C, 15 min) to concentrate the separated proteins. The protein pellet was resuspended in Buffer A, and the suspension was heat-treated at 60°C for 25 min, then ultra-centrifuged (300,000 × g, 25°C, 1 h) to remove heat-labile proteins (8). After heat-treatment, proteins were concentrated and purified using an Amicon Ultra-4, 10 kDa ultracentrifuge-type filter (Millipore, Billerica, MA, USA) (four spins at 4,000 rpm, 7°C, 15 min).

Hydrogenase activity assay

The H_2 evolution activity of the hydrogenase was assayed by the production of H_2 from methyl viologen reduced by sodium dithionite. In a 4 mL vial, 1 mL of enzyme solution and 100 μL of 25 mM methyl viologen were allowed to degas in a N_2 atmosphere. The reaction was catalyzed by adding 0.2 mL of 230 mM sodium dithionite. H_2 evolution was measured every 10 minutes from 10 to 80 minutes using a gas chromatograph (Agilent Technologies, Santa Clara, CA, USA). The evolution rate was calculated according to the slope of the reaction. The protein concentration was determined by the Lowry method using a protein assay kit (Bio-Rad, Hercules, CA, USA). Bovine serum albumin was used as the standard (8).

Results

The optical density (OD) of the culture at 650 nm before harvesting was 0.248. The culture grew for approximately three weeks to reach this density. The total wet weight of harvested cells was approximately 37 g. The hydrogen activity and protein assay data at each step are shown in Fig. 1-1 through Fig. 1-7 and Tables 1-1 through 1-5.

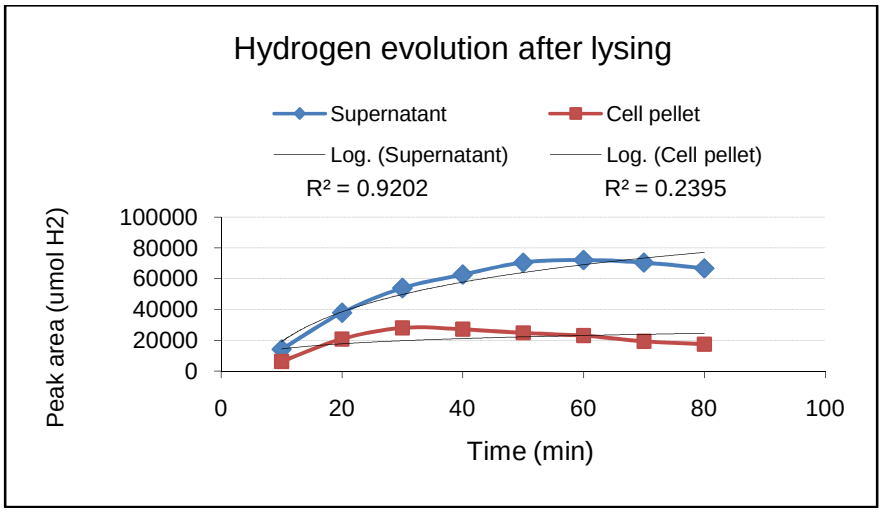

FIG.. 1-1. Hydrogen evolution data for supernatant and cell pellet fractions after initial lysing step.

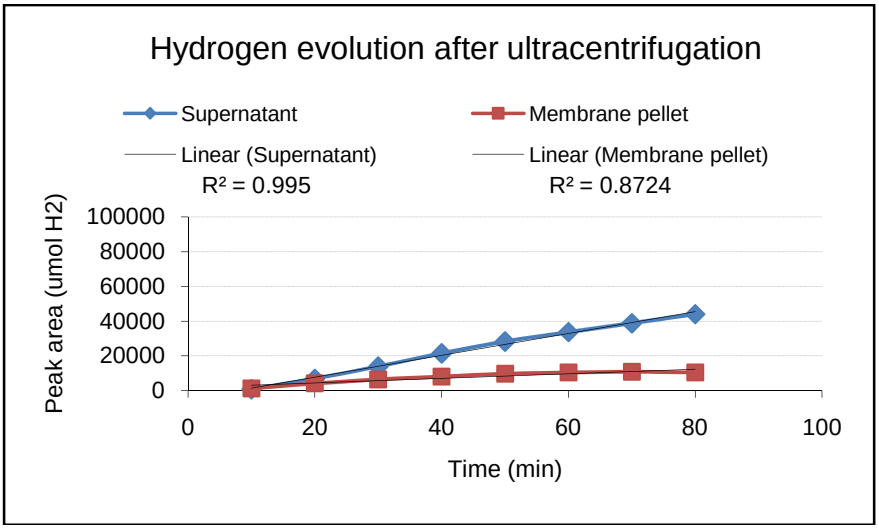

FIG. 1-2. Hydrogen evolution data for supernatant and membrane pellet fractions after ultracentrifugation step.

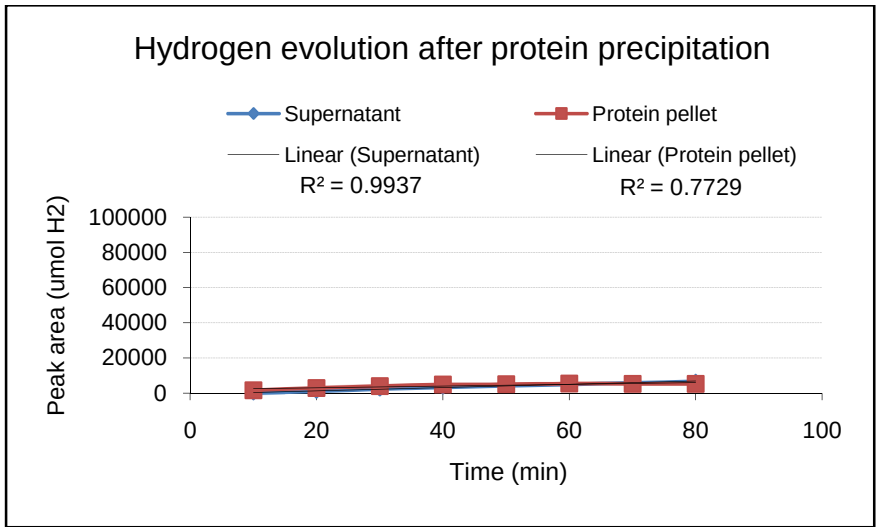

FIG. 1-3. Hydrogen evolution data for supernatant and protein pellet fractions after protein precipitation step.

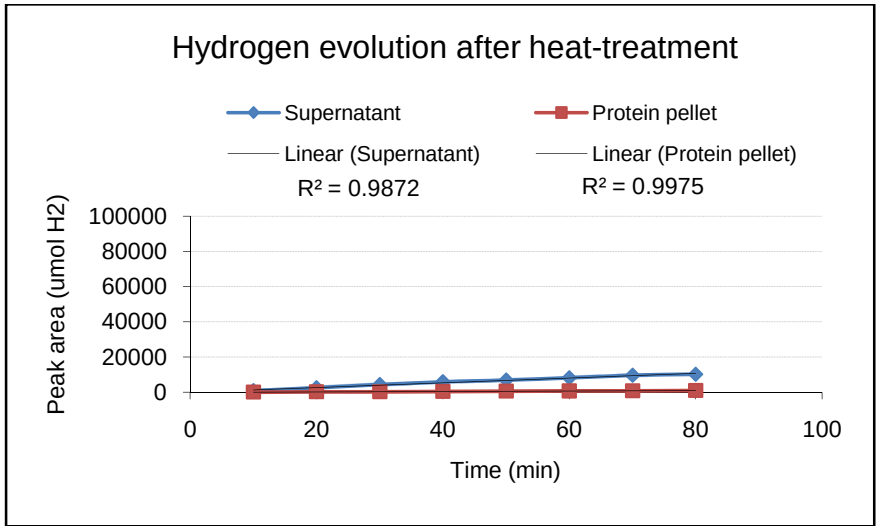

FIG. 1-4. Hydrogen evolution data for supernatant and protein pellet fractions after heat-treatment step.

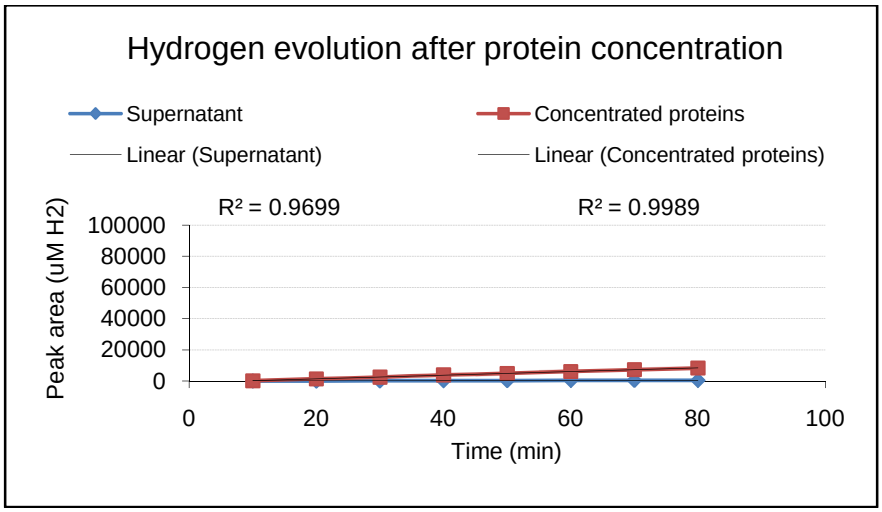

FIG. 1-5. Hydrogen evolution data for supernatant and concentrated protein fractions after final protein concentration step.

TABLE 1-1. Results of protein assays. The entire supernatant fraction from the ultracentrifugation step was used for the protein precipitation step, so nothing was available for the protein assays that were performed after the purification process on the preserved fractions.

Step	*Fraction*	*Protein (mg)*	*Total protein (mg)*
Lysing	Supernatant	1.636755	2.881371
	Cell pellet	1.244616	
Ultracentrifugation	Supernatant		
	Membrane pellet	1.856604	
Protein precipitation	Supernatant	0.263819	1.362168
	Protein pellet	1.098349	
Heat treatment	Supernatant	0.48636	0.672111
	Protein pellet	1.8575	
Concentration	Supernatant	0.0001	0.5791
	Concentrated proteins	0.579	

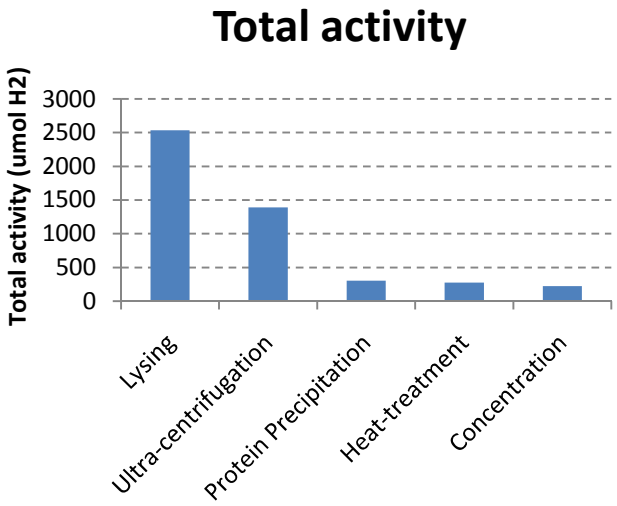

FIG. 1-6. Accumulated hydrogen evolution activity data for each step in the purification process.

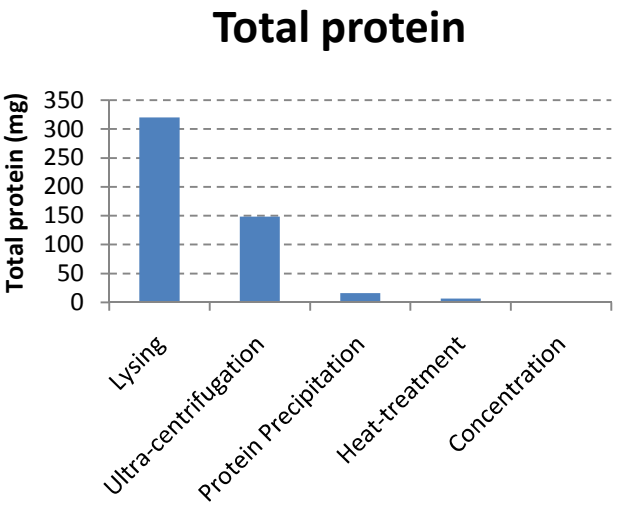

FIG. 1-7. Total protein amounts (both fractions) for each step in the concentration process.

The lysing fraction had the greatest hydrogen-evolving activity (Fig. 1-1) and protein content (Table 1-1) of all the concentration steps, because at this point all hydrogenases were active and no proteins had been removed. The supernatant at this step had higher hydrogen-evolving activity than did the cell pellet, partly because the soluble

nature of the hydrogenase caused it to remain in the cytosolic fraction (Table 1-1). The logarithmic appearance of both supernatant and cell pellet hydrogen evolution curves may be due to enzymatic inhibition as a result of high concentrations of the reaction product (H_2). After this step, the pellet of cell debris was frozen and the supernatant was used for the remaining steps since the target hydrogenase was cytoplasmic, not membrane-bound.

Hydrogen evolution after concentration by ultracentrifugation was not as high for either fraction as in the previous step (Fig. 1-2).

After precipitating out proteins by ammonium sulfate fractionation, the amount of hydrogen evolved decreased dramatically from the previous step (Fig. 1-3). As shown in Table 1-1, the protein pellet contained almost four times as much protein as did the supernatant, but both fractions had similar hydrogen evolution values, indicating that the supernatant contains the most active hydrogenases, although not necessarily the target hydrogenase.

Heat-treatment was performed using the precipitated proteins from the previous step. About half of the protein was lost between the heat-treatment step and the precipitation step (Table 1-1). Approximately 86% of the protein was retained between the concentration step and the heat-treatment step.

Fig. 1-7 shows the total amount of protein in both fractions (supernatant and pellet) for each step, determined using Lowry Standard Assay procedures. The volume-corrected amount of protein in the first (lysing) step was 319 mg, which decreased to 0.58 mg in the final step.

Discussion

Approximately one tenth of the total hydrogen-evolving activity was retained throughout the concentration process; beginning activity was 2536 µmol H_2 and ending activity was 222 µmol H_2 (Fig. 1-6). Hydrogenase activity was very well conserved in the last three concentration steps (Fig. 1-6), with hardly any loss of activity, despite decreasing protein content (Fig. 1-7). About one fifth of the total non-membrane bound activity was retained after removal of the membrane fraction by ultracentrifugation.

T. roseopersicina has many hydrogenases, but about one third of the target (non-membrane bound) proteins were retained in the concentration process. The goal of this project was to isolate and concentrate an exceptionally stable hydrogenase from *T. roseopersicina*. The high hydrogen-evolution activity after heat-treatment, which was conserved in the final steps despite loss of protein in the sample (Fig. 1-6 and Fig. 1-7), indicates successful concentration of a fairly pure thermotolerant hydrogenase of *T. roseopersicina.* Heat-treatment should have removed the activity of labile hydrogenases. However, the conservation of activity after the heat-treatment step (Fig. 1-6) indicated that the precipitation step was successful at removing the labile hydrogenases. This is supported by the large drop in activity after the precipitation step (Fig. 1-6).

Future work could include running an SDS-PAGE gel with the concentrated proteins to confirm that the sample contains only the target hydrogenase proteins.

CHAPTER 2: METHANE HYDRATES AND GRAIN SIZE PROXIES

Introduction

Gas hydrate is an icelike compound that contains methane and other low-molecular weight gases in a lattice of water molecules (14). Gas hydrates in seafloor sediments typically occur within a gas occupancy zone approximately 50 to 130 meters below sea floor (mbsf), with the maximum depth at a site strongly dependent on water depth and geothermal gradient (16). In some places, where methane-rich fluids are advected to the seafloor, massive hydrate deposits can form at the seafloor.

The main significance of hydrate is as a potential energy source and hydrocarbon sink influencing climate change. Expedition 311 (Exp311) of the International Ocean Drilling Program (IODP) was designed to study the occurrence of gas hydrates in a subduction zone accretionary complex and the processes that lead to gas hydrate formation. The expedition took place in September-October of 2005 in the northeastern Pacific Ocean near Vancouver Island, Canada. It served as a follow-up to earlier drilling cruises in 1992 and 2002 to study gas hydrates in the accretionary complex of the Cascadia subduction zone offshore of Oregon and Vancouver Island.

Observations made during Exp311 indicated that gas hydrate occurrence is closely related to the presence of coarse-grained sediments like sands. The ultimate goal of this project was to quantify this observation by measuring the grain size distribution, comparing grain size to the gas hydrate content of the sediment obtained by other means. Another goal was to measure the correlation of grain size with other, more easily measured, sediment properties.

The initial preparation of samples was conducted on board Exp311 as part of the procedure to determine the density and porosity of the samples. The shipboard analysis, which was done by Dr. Trehu and colleagues in the Physical Properties group, entailed picking samples every 50-100 cm along the hundreds of meters of sediment core that were recovered. Cores were drilled in a transect along the accretionary prism at Sites 1325, 1326, 1327, 1328 and 1329. The Moisture and Density group (MAD) samples were weighed before and after being dried and the volumes were measured. Analysis was performed with the residue from these samples. Another set of samples was also taken with adjacent MAD samples and was not dried on board the ship. Due to labeling codes, these unbaked samples were labeled "ATSED." The purpose of comparing ATSED and adjacent MAD samples was to determine what (if any) effects drying had on the samples. In the case of significant differences between the percent of sand or clay in an ATSED and its adjacent MAD sample, photos of the cores served as references to determine whether the heterogeneity was real or a result of the drying process.

The main objective of this project was to evaluate different sediment parameters as proxies for grain size; such proxies would enable grain size in sediments to be estimated for past cruises and future work using easily-gathered parameters. The parameters used were: porosity, a measure of the void spaces in sediment; bulk density, the mass of sediment per unit volume; grain density, the dry weight of sediment material divided by the grain volume; and magnetic susceptibility, the degree to which material can be magnetized in an external magnetic field. These and other proxies have been used to predict sediment grain size in other studies. For example, acoustic compressional wave velocity (acoustic velocity) has been used as a predictor of physical and elastic properties

of soils, sediments and rocks since the 1950s (11). More recently, this method was used to predict grain size in glacio-marine sediments (11). Unfortunately, the acoustic velocity could not be easily measured in the gaseous sediments from Exp311. Properties such as density and magnetic susceptibility have also been used as grain size proxies to indicate the presence of paleo-earthquake activity, with results showing good correspondence between these properties and grain size (7).

Validation of analysis methods was performed by comparing grain size measurement techniques to determine the most accurate method. Dried sediment samples were analyzed by dry-sieving, wet-sieving, or using a Coulter LS 100Q Laser Diffraction Particle Size Analyzer (LDPSA). Included within this validation objective was analysis to determine the effect of drying on the samples. To achieve this, grain size was analyzed and compared between ATSED and adjacent MAD samples.

One important application for this grain size analysis is to determine the relationship between grain size and gas hydrate content within core samples. Grain size analysis was performed using the LDPSA, and gas hydrate analysis was performed by the Interstitial Waters (IW) group of Exp 311. (See Appendix for full report, including methods, results and conclusions.)

Materials and Methods

Validation of analysis methods

All analyzed samples were characterized as either friable (“crumble easily”), which had already dissociated or crumbled easily to the touch; firm (“fall apart”), which fell apart with moderate finger pressure or had partially dissociated; and solid (“unanalyzed”), which did not fall apart with any amount of pressure unless chipped

apart. Samples that crumbled easily were generally found to have a higher sand content than those that were firm or solid. A few solid samples were analyzed via wet-sieving and the sand content was 0%. For this reason, all solid samples were assumed to have a negligible amount of sand and were not wet-sieved.

In order to determine the percentage volume of >125 μm (coarse sand), 63-125 μm (fine sand), and <63 μm (silt and clay) fractions in a given sample, three methods were used: dry-sieving, wet-sieving, and analysis with the LDPSA. MAD samples were identified using a number system, while ATSED samples were labeled using a letter system.

For dry-sieving, a 125 μm sieve (USA Standard Series No. 120) was placed on top of a 63 μm sieve (No. 230) and both were placed on top of a 400 mL beaker. The sample was poured in the No. 120 sieve and distributed evenly through the sieves by rotating and gently shaking the stacked sieves and beaker. For MAD samples #4-7, a rubber policeman spatula was used to brush grains along the mesh to ensure all appropriate particles were sieved. Only MAD samples #1-7 were partially dry-sieved.

For wet-sieving, liquid was added to each sample to be analyzed and the samples were left to soak overnight or for at least one hour. At the beginning of wet-sieving analysis, 50 mL of deionized (DI) water was used as the liquid, but later a chemical dispersant solution was used (58.4 mM $(NaPO_3)_6$, 74.9 mM Na_2CO_3 in DI H_2O; J.H. Power, US EPA).

After soaking, the beakers were placed in an ultrasonic shaker for 60 minutes. Using a wash bottle filled with DI water, each sample was individually washed through No. 120 and No. 230 sieves. The <63 μm (fine) fraction was collected and set aside. The

remaining two fractions were each separately drained of water using a vacuum pump and filter paper. These were then transferred to appropriately labeled foil weighing dishes which were placed in a convection oven set to 60°C for at least 24 hours. After drying, the samples were transferred to a dessicator to cool. The mass of each fraction was recorded. Over 600 samples were analyzed by wet-sieving.

A subset of the sediment samples was analyzed with the LDPSA. This was used to verify the accuracy and analyze particle size in the previously sieved samples MAD samples #1-15, as well as MAD samples #16-65 and ATSED samples #M-O, which had not previously been sieved. Procedure for this analysis can be found in: EPA SOPPMP.04 (Power, J. H. 2003. Measurement of sediment grain size distribution using a laser diffraction particle size analyzer. EPA SOPPMP.04, unpublished report). Access limitations precluded the use of the LDPSA to analyze all MAD samples, so it was used mainly to verify the accuracy of sieving.

MAD samples #1-7 were divided into two parts. One part was dry-sieved and the other wet-sieved in order to determine the precision of dry- versus wet-sieving. For MAD samples #8-15, approximately half of the original sample was removed for wet-sieving, and the rest of the sample was preserved for future analysis. This procedure was also followed for ATSED and adjacent MAD samples #A-L. ATSED samples #M-O did not have adjacent MAD samples and were only analyzed using the LDPSA.

Calibration of Laser Diffraction Particle Size Analyzer

Three samples of glass beads were created, using beads of size 37-53 µm, 105-149 µm, and 297-420 µm, to calibrate the data produced by the LDPSA. The mass percent of each size range in each of the three samples is shown in Table 2-1.

TABLE 2-1. Percentage of each glass bead size fraction in glass samples.

	37-53 µm	105-149 µm	297-420 µm
Glass 1	33%	34%	33%
Glass 2	13%	36%	51%
Glass 3	57%	28%	15%

Each glass bead sample was run in the machine using the same method as other sediment samples. Fig. 2-1 - Fig. 2-3 show the results of these analyses. The large variability between individual runs (displayed as different colored lines in each readout, with the black line as the average of all runs) indicate slightly less precision in samples with larger percentages of sand-sized particles (>63 µm). It appears to be largely the percent of sand-sized particles in a sample, and less the actual size of the particles themselves, that accounts for a decrease in precision between runs. In only a few cases, greater variability in analyses was due to a high obscuration (>12%) within the machine, which impedes the ability of the machine to analyze samples accurately.

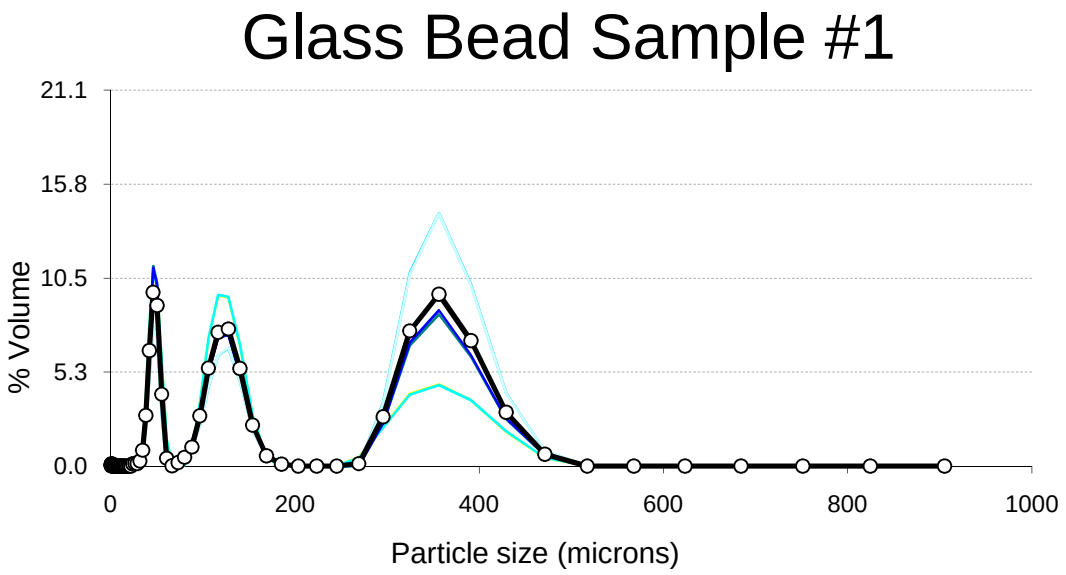

FIG. 2-1. Analysis of glass bead sample #1 (Glass 1). The composition of this sample was: 33% 37-53 µm, 34% 105-149 µm, and 33% 297-420 µm. The multiple colored lines represent the results from each of the six "runs" the LDPSA conducts for each individual sample. The thick black line represents the average of all runs.

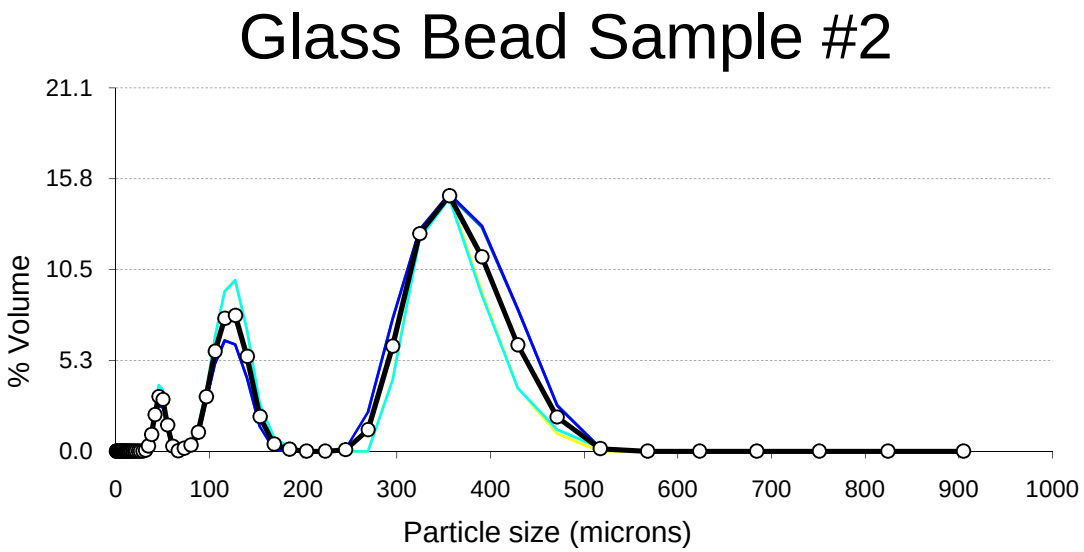

FIG. 2-2. Analysis of glass bead sample #2 (Glass 2). The composition of this sample was: 13% 37-53 µm, 36% 105-149 µm, and 57% 297-420 µm. The multiple colored lines represent the results from each of the six "runs" the LDPSA conducts for each individual sample. The thick black line represents the average of all runs.

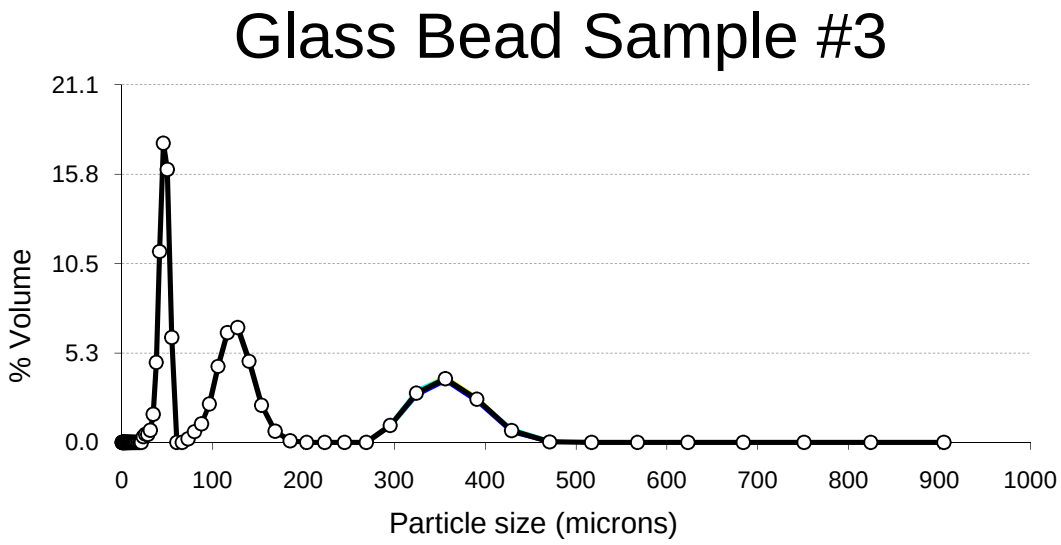

FIG. 2-3. Analysis of glass bead sample #3 (Glass 3).The composition of this sample was: 57% 37-53 µm, 28% 105-149 µm, and 15% 297-420 µm. The multiple colored lines represent the results from each of the six "runs" the LDPSA conducts for each individual sample. The thick black line represents the average of all runs.

TABLE 2-2. Percentage total of each size range within glass bead samples. The first row for each sample represents the total calculated by the LDPSA. The second row represents the total when the size range was manually expanded to include grains from 34.584-55.135 µm, 96.491-153.283 µm, and 295.524-429.168 µm. The third row represents the actual total when the samples were created.

Sample Name		297-420 µm fraction	105-149 µm fraction	37-53 µm fraction	Total
Glass 3	LDPSA:	24.220	26.127	28.045	78.393
	Expanded:	29.991	31.250	32.957	94.198
	should be:	33.000	34.000	33.000	100.000
Glass 2	LDPSA:	38.678	26.853	9.253	74.783
	Expanded:	50.933	32.016	11.066	94.014
	should be:	51.000	36.000	13.000	100.000
Glass 1	LDPSA:	9.198	22.468	49.614	81.280
	Expanded:	10.900	26.921	57.454	95.275
	should be:	15.000	28.000	57.000	100.000

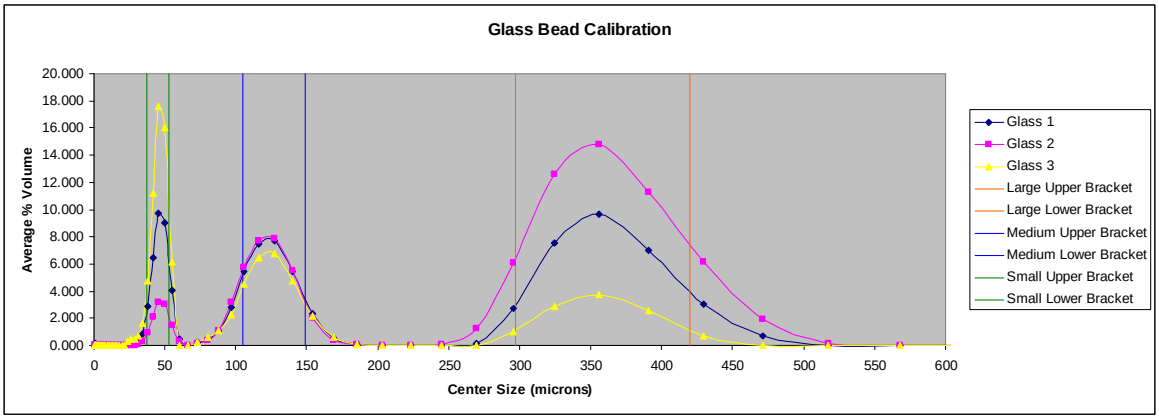

FIG. 2-4. Comparison of all glass bead samples according to size range. The largest spread occurs in Glass 2 (which had the highest percentage of large particle sizes) around the 297-420 µm size range.

Comparison of the three glass bead graphs (Fig. 2-1 - 2-3) is shown in Fig. 2-4, which also shows the size ranges the distributions should fit within. The peaks are discrete and correspond well to the labeled size ranges of glass beads. There is far less spread in the small (37-53 µm) size range than in the medium (105-149 µm) and large (297-420 µm) size ranges. The largest amount of spread occurs in Glass 2, which had the highest amount of large particles, in the 297-420 µm range. This suggests higher uncertainty for samples with larger grain sizes, a trend that can be seen in the graphs

resulting from analysis of IW 13a and IW 13b especially (which each contained particles larger than 850 µm), although there are other samples that show this quality as well. The smooth, precise nature of the percentage volume curves generated during the glass bead calibration probably indicates a certain amount of "smoothing" by the LDPSA of the data gathered.

Grain size proxy analysis

The other sediment parameters used in grain size proxy analysis were measured on shipboard as part of the standard IODP analysis sequence. Grain size analysis was performed for samples from all drilling sites using wet-sieving, with additional LDPSA analysis for MAD samples #1-15 and ATSED and MAD samples #A-O. All samples were disaggregated using dispersant solution with the exception of MAD samples #51, 59-65, which were soaked in DI water.

Results

Validation of analysis methods

Fig. 2-5 details results from the comparison between dry-sieving and wet-sieving for MAD samples #1-7. The data illustrate the bias towards larger grain sizes of the dry-sieving technique. Dry-sieving was abandoned on the basis of these results.

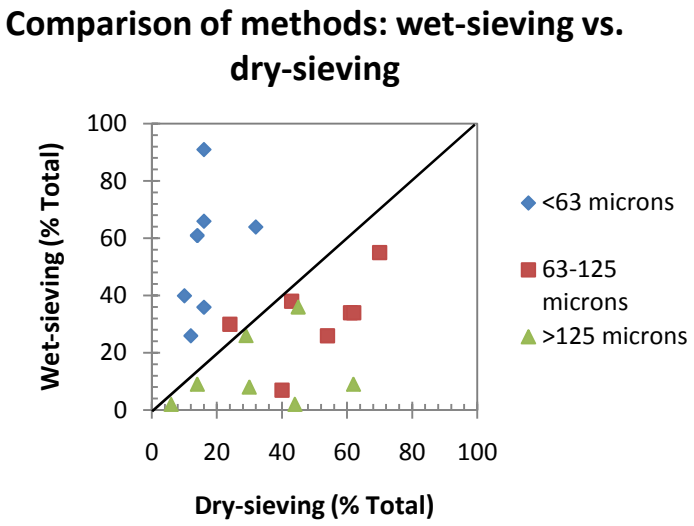

FIG. 2-5. Comparison of wet-sieving vs. dry-sieving methods.The diagonal indicates where points should lie if dry-sieving and wet-sieving totals were equivalent. Points below the line indicate bias in the dry-sieving method, while points above it indicate a bias in the wet-sieving method.

LDPSA analysis was performed to test the accuracy of wet-sieving. A total of 154 IW, MAD, and ATSED samples were analyzed by LDPSA. Of these, 39 had been wet-sieved prior to LDPSA analysis. Overall, in the 15 MAD samples that were both wet-sieved and analyzed by the LDPA, wet-sieving resulted in similar percent volumes (within 20%) of various grain sizes to those in the LDPSA analysis (Figure 2-6).

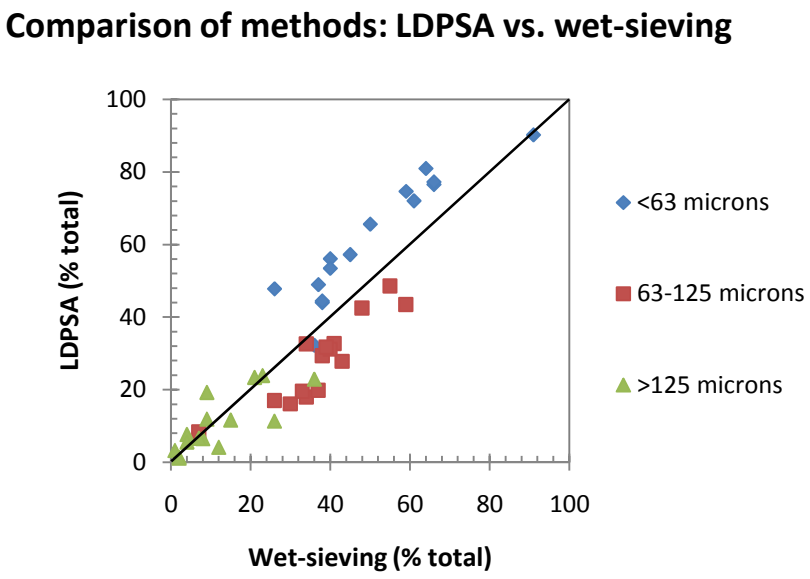

FIG. 2-6. Comparison of LDPSA analysis vs. wet-sieving. These data show a segregation of silt and clay (<63 μm) particles and fine sand (63-125 μm) particles.

The data for the comparison of ATSED and adjacent MAD samples also show a comparison between LDPSA and wet-sieving analyses (Table 2-3). As in the comparison between dry- and wet-sieving, the differences between LDPSA and wet-sieving were within 20% of the total for each grain size fraction. Aside from a few anomalies, such as ATSED and MAD A and C, the difference in grain size fractions was usually within 6% for the LDPSA and 10% for wet-sieving. The reason for discrepancies within anomalous ATSED and MAD samples A and C can be seen in Fig. 2-11 and 2-12.

TABLE 2-3. Percent grain size fraction for ATSED and adjacent MAD samples for LDPA and wet-sieving analyses.

	LDPSA (% total)			Wet-sieving (% total)		
	>125 μm	63-125 μm	<63 μm	>125 μm	63-125 μm	<63 μm
ATSED A	14.037	36.895	49.068	9	22	69
MAD A	1.098	5.989	92.913	2	12	86
ATSED B	0.075	0.421	99.504	0	0	100
MAD B	0.002	0.214	99.783	0	0	100
ATSED C	0.834	2.628	96.538	0	1	99
MAD C	1.256	4.175	94.569	0	8	92
ATSED D	0.129	0.994	98.877	0	0	100
MAD D	0.002	0.109	99.889	0	0	100
ATSED E	0.010	0.278	99.713	0	0	100
MAD E	0.051	0.555	99.393	0	0	100
ATSED F	1.246	3.420	95.334	0	1	100
MAD F	0.386	1.325	98.290	0	1	100
ATSED G	5.803	24.819	69.378	1	19	80
MAD G	3.241	21.383	75.376	1	30	69
ATSED H	2.141	11.081	86.777	1	10	89
MAD H	2.012	19.011	78.977	0	27	73
ATSED i	0.079	0.529	99.392	0	0	100
MAD i	0.131	1.044	98.825	0	0	100
ATSED J	1.548	5.149	93.303	0	1	99
MAD J	0.807	8.245	90.948	0	6	94
ATSED K	0.476	2.366	97.159	0	1	99
MAD K	2.258	12.843	84.899	0	9	91
ATSED L	0.017	0.212	99.771	0	0	100
MAD L	0.043	0.298	99.659	0	1	99
ATSED M	2.983	17.188	79.829			
ATSED N	0.084	0.814	99.102			
ATSED O	0.183	0.758	99.059			

Grain size proxy analysis

Several sediment parameters were tested for correlation with grain size. Porosity showed almost no correlation to grain size as measured in sand content (Fig. 2-7). It has been established for marine sediments that as grain size decreases, porosity increases (11). This trend can be seen more clearly for samples that fall apart easily, which generally had a smaller percentage of sand >125 μm than the samples that crumbled easily (Fig. 2-7).

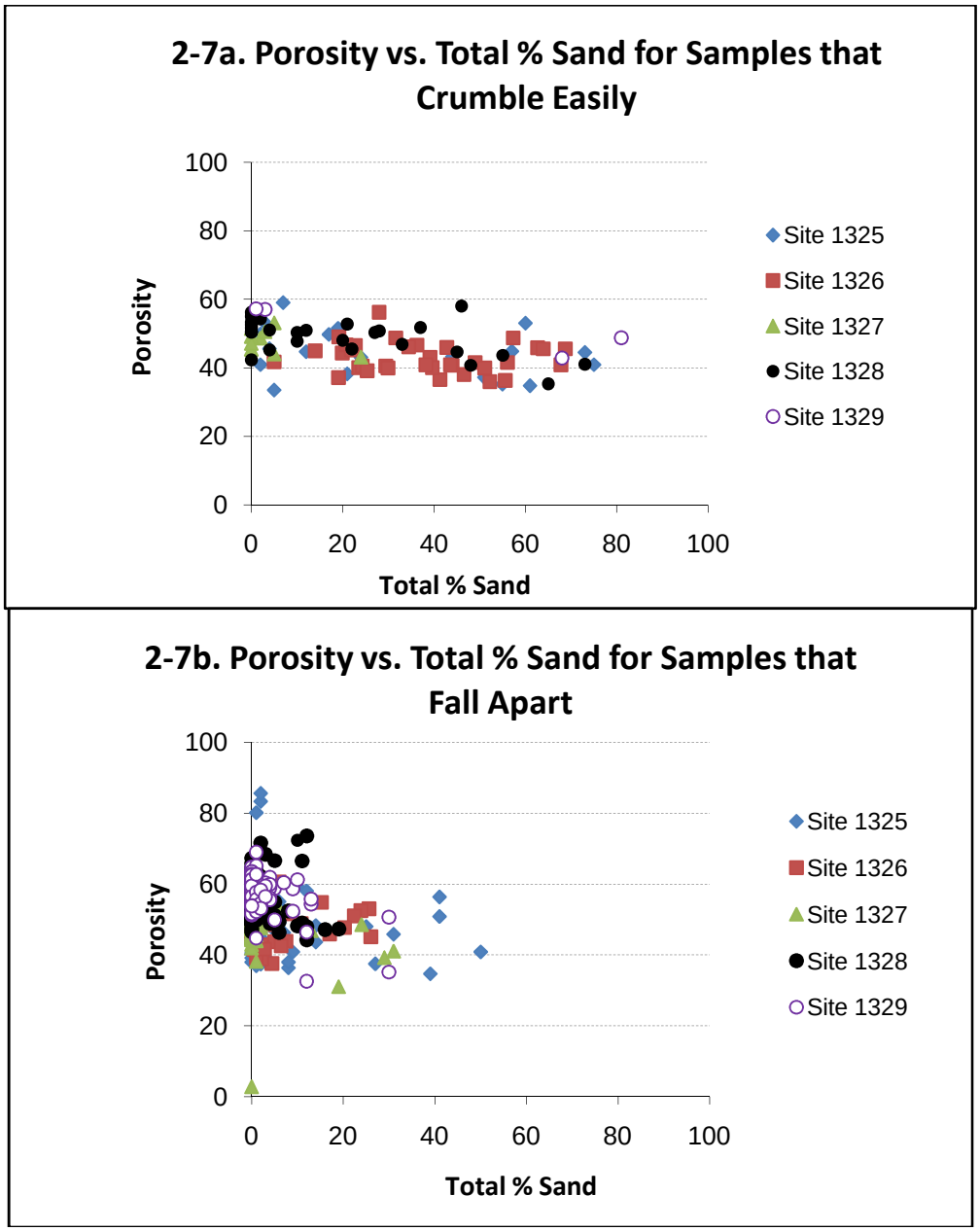

FIG. 2-7. Porosity vs. total % sand per sample graphed for all five coring sites.

TABLE 2-4. Statistics for Fig. 2-7a. The *n* column represents the number of samples that crumble easily that were analyzed for a particular site.

Porosity vs Total % Sand for Samples that Crumble Easily				
Site	**Slope**	**Intercept**	**R^2**	**n**
1325	-0.0849	46.883	0.1017	23
1326	-0.0353	44.198	0.0175	36
1327	-0.2228	48.999	0.2509	9
1328	-0.1366	51.737	0.3365	28
1329	-0.1469	57.043	0.7881	5
All Sites	-0.0517	47.222	0.084	101

TABLE 2-5. Statistics for Fig. 2-7b. The *n* column represents the number of samples that fall apart that were analyzed for a particular site.

Porosity vs Total % Sand for Samples that Fall Apart				
Site	**Slope**	**Intercept**	**R^2**	**n**
1325	-0.1217	49.939	0.0183	117
1326	0.028	48.722	0.0016	52
1327	-0.2932	49.36	0.0549	110
1328	-0.1441	55.287	0.0089	80
1329	-0.5368	58.507	0.2547	107
All Sites	-0.2072	52.589	0.0328	466

Magnetic susceptibility proved slightly more useful than porosity as a proxy for grain size, but mostly for samples with a high sand content (Fig. 2-8 and Table 2-6). Overall, there was very little correlation between magnetic susceptibility and sand content (Tables 2-6 and 2-7).

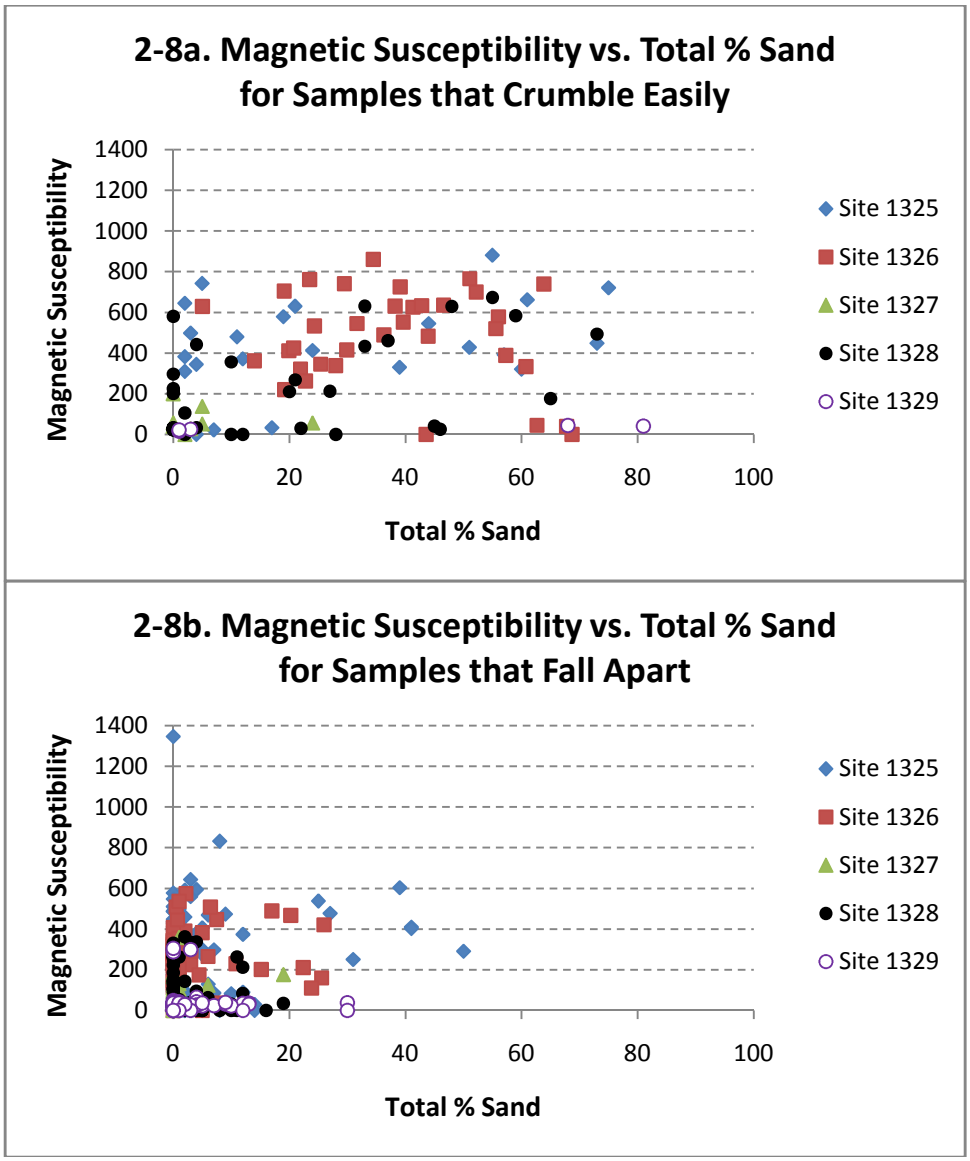

FIG 2-8. Total % sand per sample vs. magnetic susceptibility graphed for all coring sites.

TABLE 2-6. Statistics for Fig. 2-8a. The *n* column represents the number of samples that crumble easily that were analyzed for a particular site.

Magnetic Susceptibility vs Total % Sand for Samples that Crumble Easily				
Site	**Slope**	**Intercept**	**R^2**	**n**
1325	2.9821	358.65	0.1141	23
1326	-3.2074	589.28	0.0486	36
1327	-0.9137	76.134	0.0125	9
1328	4.7398	133.68	0.2176	31
1329	0.2803	22	0.8776	5
All Sites	3.6039	238.27	0.1041	104

TABLE 2-7. Statistics for Fig. 2-8b. The *n* column represents the number of samples that fall apart that were analyzed for a particular site.

Magnetic Susceptibility vs Total % Sand for Samples that Fall Apart				
Site	**Slope**	**Intercept**	**R^2**	**n**
1325	4.0538	223.04	0.0274	117
1326	0.3492	279.54	0.0004	51
1327	5.9847	50.591	0.0541	110
1328	-3.7905	94.901	0.0223	81
1329	-0.7815	39.574	0.0041	107
All Sites	4.881	117.5	0.0336	466

Neither bulk density nor grain density showed any promising correlation with grain size.

Figures 2-9 and 2-10 show graphs of grain density and bulk density from all sites, and

Tables 2-8 through 2-11 show relevant statistics.

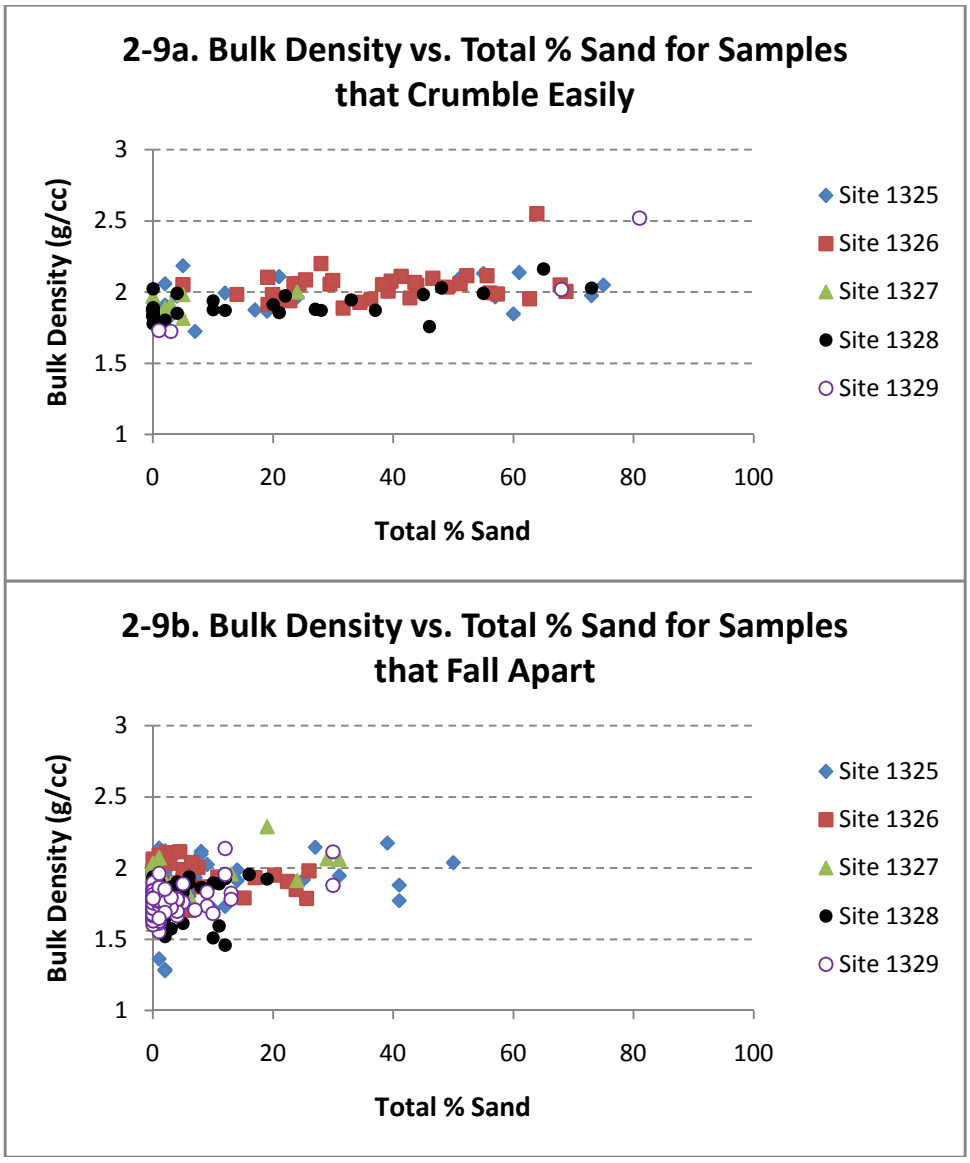

FIG. 2-9. Graphs of bulk density vs. total % sand per sample for all coring sites.

TABLE 2-8. Statistics for Fig. 2-9a. The *n* column represents all the samples that crumbled easily that were analyzed for a particular site.

Bulk Density vs Total % Sand for Samples that Crumble Easily				
Site	**Slope**	**Intercept**	**R²**	**n**
1325	0.0013	1.9454	0.0804	23
1326	0.002	1.9676	0.0804	36
1327	0.0036	1.9045	0.2113	9
1328	0.0023	1.8608	0.3172	28
1329	0.008	1.695	0.8084	5
All Sites	0.0031	1.8909	0.2911	101

TABLE 2-9. Statistics for Fig. 2-9b. The *n* column represents all the samples that fall apart that were analyzed for a particular site.

Bulk Density vs Total % Sand for Samples that Fall Apart				
Site	**Slope**	**Intercept**	**R²**	**n**
1325	0.0022	1.889	0.0189	113
1326	-0.001	1.921	0.0061	50
1327	0.0064	1.8857	0.1103	110
1328	0.0013	1.802	0.0024	80
1329	0.0094	1.7306	0.239	107
All Sites	0.0038	1.8383	0.0377	460

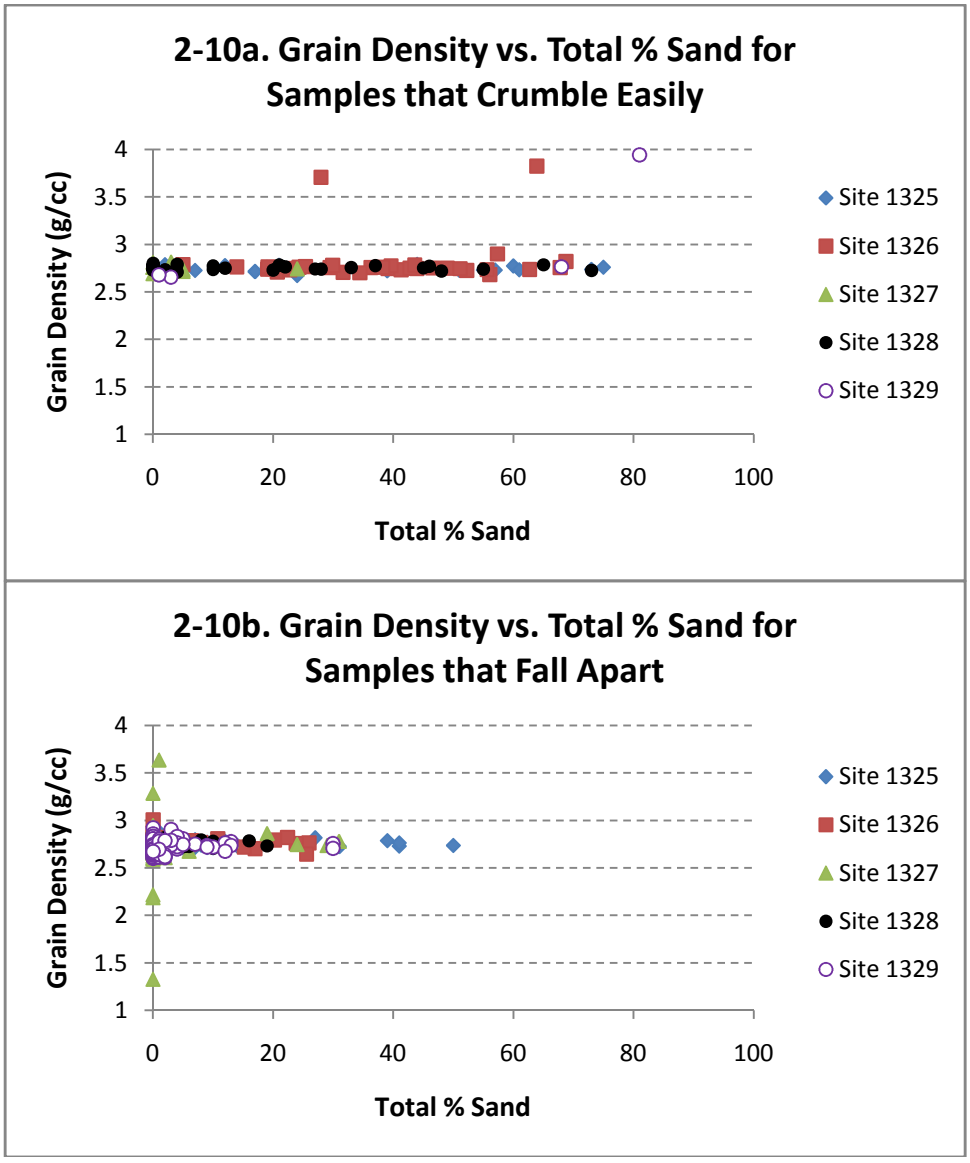

FIG. 2-10. Graphs of grain density vs. total % sand per sample for all coring sites.

TABLE 2-10. Statistics for Fig. 2-10a. The *n* column represents the number of samples that crumble easily that were analyzed for a particular site.

Grain Density vs Total % Sand for Samples that Crumble Easily				
Site	**Slope**	**Intercept**	**R^2**	**n**
1325	-0.00002	2.7574	0.0454	23
1326	0.0023	2.7252	0.0248	36
1327	-0.0006	2.7508	0.0108	9
1328	-0.0001	2.7578	0.0134	28
1329	0.0108	2.5993	0.5296	5
All Sites	0.002	2.7275	0.0604	101

TABLE 2-11. Statistics for Fig. 2-10b. The *n* column represents the number of samples that fall apart that were analyzed for a particular site.

Grain Density vs Total % Sand for Samples that Fall Apart				
Site	**Slope**	**Intercept**	**R^2**	**n**
1325	-0.0005	2.7637	0.0136	113
1326	-0.0011	2.7723	0.0224	50
1327	0.0022	2.7294	0.0033	110
1328	-0.0028	2.7654	0.0851	80
1329	0.0007	2.7259	0.003	107
All Sites	0.0002	2.7461	0.0002	460

Discussion

Validation of analysis methods

Dry-sieving was conducted as a test of sieving methods. Because it is faster, dry-sieving would have been more convenient for processing the hundreds of sediment samples recovered from the cruise. The comparison of dry-sieving versus wet-sieving shows marked differences between the two sets of results (Fig. 2-5). The clear segregation between sand sized (>63 μm) fractions below the line and smaller (<63 μm) fractions above the line suggest that there is a bias in the dry-sieving method towards larger grain sizes (Fig. 2-5). After completing these samples, it was determined that dry-sieving was less accurate, possibly because electrostatic forces between smaller grains led

to a consistent bias towards larger grain sizes, and dry-sieving was discontinued in favor of wet-sieving the remaining samples.

LDPSA analysis usually shows larger amounts of silts and clays, while wet-sieving usually gives a higher percentage of fine sands (Fig. 2-6). There may be several reasons for discrepancies between the wet-sieving and LDPSA analyses (Fig. 2-6). First, the LDPSA may be more accurate than is wet-sieving. The use of a chemical dispersant in the LDPSA procedure may also have an advantage over the DI water used in the wet-sieving procedure, although to counter this effect, the dispersant solution was used in later wet-sieving samples.

The two procedures may also have different biases. Because of human error and the incomplete disaggregation of sediments, wet-sieving is more likely to have been biased towards larger grain sizes. Conversely, because of properties of the agitator used to stir sediment samples, the LDPSA may have been biased towards smaller grain sizes in samples with larger percentages of sand. The agitator is essentially a propeller that extends almost to the bottom of a beaker containing RO water and about 1.5 g of the sample to be analyzed. In samples with higher sand content or larger (coarse sand-sized) grains, smaller grains were suspended by the motion of the agitator propeller while some of the largest grains fell out of suspension and collected under the spinning propeller where they could not be pipetted for analysis in the LDPSA. At the very least, there was generally less precision in the results obtained in an analysis when particle sizes approach ~300 μm. This was evident in an analysis of glass bead samples by the machine. For this reason, it is recommended that samples for the LDPSA first be sieved to remove the grain size fraction larger than 300 μm. Other biases may be due to characteristics of the

LDPSA software, specifically the assumption that all particles are spherical and the smoothing function apparent during the glass bead calibration.

Ultimately, the most accurate method of grain size analysis was the LDPSA. Wet-sieving was determined to be a comparable and more convenient technique and was used for the bulk of grain size analysis for all coring sites.

Overall, ATSED results were determined to be homologous to adjacent MAD samples in percent of grain size fractions (Table 2-3). There was a marked difference between the percentage total sand fraction (63-125 μm) in ATSED and adjacent MAD samples #A and #C (Table 2-3). This difference appeared to be explained by real heterogeneity in the samples (Fig. 2-11 and 2-12). ATSED #A appeared to be located in a part of the core with much larger sand fraction than MAD #A (Fig. 2-11). The same appeared to be true for ATSED and adjacent MAD sample #C (Fig. 2-12). The adjacent MAD sample displayed a larger sand fraction because it was taken from a part of the core with more sand than the ATSED sample. These results demonstrated that drying samples makes very little difference in the analysis of samples.

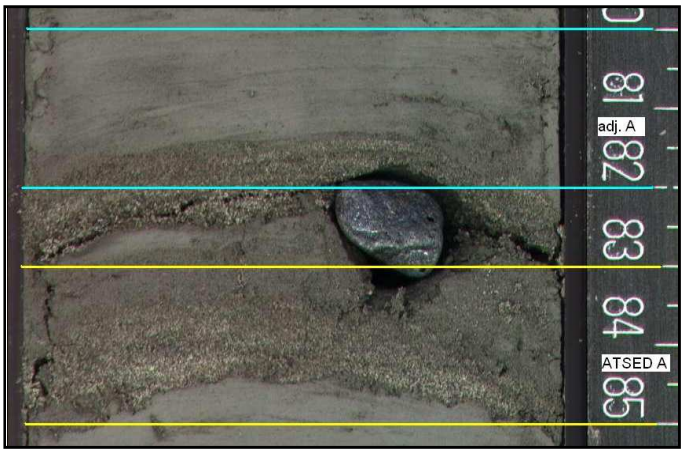

FIG. 2-11. Core photograph of ATSED and adjacent MAD sample #A. The pebble located between the two samples is likely from glacial deposit.

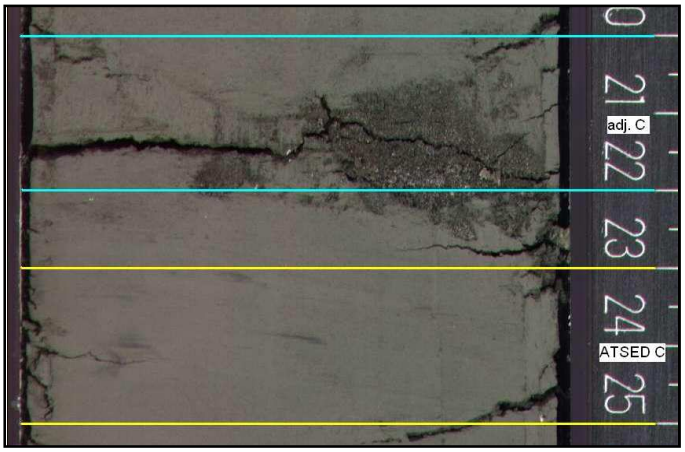

FIG. 2-12. Core photograph of ATSED and adjacent MAD sample #C.

Grain size proxy analysis

Overall, none of the sediment parameters showed significant correlation to grain size that would enable them to be used as effective proxies. Porosity showed no distinct correlation at all with grain size. Magnetic susceptibility showed a very weak correlation with grain size, but mostly for samples that had a high sand content. Both bulk density and grain density showed almost no correlation with the amount of sand per sample. These results have important implications for research involving marine sediments. Because of the poor correlation these properties had with grain size, research should continue for other, more effective proxies.

REFERENCES

1. **Adams, M. W. W. and E. I. Steifel.** 1998. Biological Hydrogen Production: Not So Elementary. Science. **282**: 1842-1843.

2. **Baek, J-S, E-H Choi, Y-S Yun, S-C Kim, and M-S Kim.** 2006. Comparison of Hydrogenases from *Clostridium butyricum* and *Thiocapsa roseopersicina*: Hydrogenases of *C. butyricum* and *T. roseopersicina.* Journal of Microbiology and Biotechnology. **16**: 1210-1215.

3. **Department of Energy.** 2008. DOE's Methane Hydrate R&D Program: Methane Hydrate- The Gas Resource of the Future. July 2008. <http://fossil.energy.gov/programs/oilgas/hydrates/ > August 2008.

4. **Energy Information Administration**. 2008. Greenhouse Gases, Climate Change & Energy. [Brochure.] <http://www.eia.doe.gov/bookshelf/brochures/greenhouse/Chapter1.htm> August 2008.

5. **Environmental Protection Agency.** 2008. Basic Information: Climate Change. April 2008. < http://www.epa.gov/climatechange/basicinfo.html> August 2008.

6. **Gogotov, I. N., N. A. Zorin, L. T. Serebriakova, and E. N. Kondratieva.** 1978. The properties of hydrogenase from *Thiocapsa roseopersicina*. Biochimica et Biophysica Acta. **523**: 335-343.

7. **Goldfinger, C., A. Morey, C. H. Nelson, J. Gutiérrez-Pastor, J.E. Johnson, E. Karabanov, J. Chaytor, A. Eriksson, and the Shipboard Scientific Party.** 2007. Rupture lengths and temporal history of significant earthquakes on the offshore and north coast segments of the Northern San Andreas Fault based on Turbidite Stratigraphy. Earth and Planetary Science Letters. **254**: 9-27.

8. **Kim, M. S., E. H. Choi, and Y. K. Oh.** 2008. Characterization of hydrogenase from purple sufur bacterium *Thiocapsa roseopersicina* and its prolonged *in vitro* hydrogen evolution. International Journal of Hydrogen Energy. **33:** 1496-1502.

9. **Kovács, K. L., G. Tigyi, and H. Alfonz.** 1985. Purification of hydrogenase by Fast Protein Liquid Chromatography and by conventional separation techniques: A comparative study. Preparative Biochemistry and Biotechnology. **15:** 321-334.

10. **Kovács, K. L., Á. T. Kovács, G. Maróti, L. S. Mészáros, J. Balogh, D. Latinovics, A. Fülöp, R. Dávid, E. Dorogházi, and G. Rákhely.** 2005. The hydrogenases of *Thiocapsa roseopersicina.* Biochemical Society Transactions. **33-1:**61-63.

11. **Moran, K., V. Altmann, M. O'Regan, and C. Ashmankas.** 2007. Acoustic Compressional Wave Velocity as a Predictor of Glacio-marine Sediment Grain Size. Geotechnical Testing Journal. **30**

12. **Pfennig, N. and H. G. Trüper.** 1992. The Family Chromatiaceae. In: Balows, A., Trüper, H.G., Dworkin, M., Harder, W. and K.H. Schleifer. (Eds.), The prokaryotes. A Handbook on the biology of bacteria: ecophysiology, isolation, identification, applications. Vol. 4. Springer, Berlin Heidelberg New York. 3200-3221.

13. **Sapra, R., M. F. J. M. Verhagen, and M. W. W. Adams.** 2000. Purification and Characterization of a Membrane-Bound Hydrogenase from the Hyperthermophilic Archaeon *Pyrococcus furiosus*. Journal of Bacteriology. **182:** 3423-3428.

14. **Su, X., C. –B. Song, and N. –Q. Fang.** 2006. Relationship between sediment granulometry and the presence of gas hydrate on Hydrate Ridge. In Tréhu, A.M., G. Bohrmann, M. E. Torres, and F. S. Colwell (Eds.), Proc. ODP, Sci. Results, 204: College Station, TX (Ocean Drilling Program), 1–30.

15. **Torres, M. E, A. M. Tréhu, N. Cespedes, M. Kastner, U. G. Wortmann, J. –H. Kim, P. Long, A. Malinverno, J.W. Pohlman, M. Riedel, and T. Collett. 2008**. Methane hydrate formation in turbidite sediments of northern Cascadia, IODP Expedition 311. Earth and Planetary Science Letters. **271**: 170-180.

16. **Trehu, A. M., C. Ruppel, G. R. Dickens, M. Holland, M. E. Torres, T.S. Collett, D. Goldberg, M. Riedel, and P. Schultheiss.** 2006. Gas hydrates in marine sediments: lessons from scientific drilling. Oceanography. **19-4**: 124-142.

17. **United Nations.** 2008. Global Issues on the United Nations Agenda. August 2008. < http://www.un.org/issues/>

18. **Upadhyay, J., and J. L. Stokes.** Temperature-sensitive hydrogenase and hydrogenase synthesis in a psychrophilic bacterium. Journal of Bacteriology. **86:** 992-998.

APPENDIX- Methane hydrate formation in turbidite sediments of northern Cascadia, IODP Expedition 311